

Dynamic analysis and performance assessment of the Inertial Sea Wave Energy Converter (ISWEC) device via harmonic balance

*Original*

Dynamic analysis and performance assessment of the Inertial Sea Wave Energy Converter (ISWEC) device via harmonic balance / Carapellese, Fabio; Pasta, Edoardo; Faedo, Nicolas; Giorgi, Giuseppe. - 55:(2022), pp. 439-444. (Intervento presentato al convegno 14th IFAC Conference on Control Applications in Marine Systems, Robotics and Vehicles (CAMS 2022) tenutosi a Lyngby, Denmark nel 14-16 September 2022) [10.1016/j.ifacol.2022.10.467].

*Availability:*

This version is available at: 11583/2973494 since: 2022-11-30T11:17:00Z

*Publisher:*

Elsevier

*Published*

DOI:10.1016/j.ifacol.2022.10.467

*Terms of use:*

openAccess

This article is made available under terms and conditions as specified in the corresponding bibliographic description in the repository

*Publisher copyright*

Elsevier postprint/Author's Accepted Manuscript

© 2022. This manuscript version is made available under the CC-BY-NC-ND 4.0 license  
<http://creativecommons.org/licenses/by-nc-nd/4.0/>. The final authenticated version is available online at:  
<http://dx.doi.org/10.1016/j.ifacol.2022.10.467>

(Article begins on next page)

# Dynamic analysis and performance assessment of the Inertial Sea Wave Energy Converter (ISWEC) device via harmonic balance

Fabio Carapellese<sup>1</sup>, Edoardo Pasta, Nicolás Faedo,  
Giuseppe Giorgi

*Marine Offshore Renewable Energy Lab., Department of Mechanical  
and Aerospace Engineering, Politecnico di Torino, 10129 Torino, Italy*

---

**Abstract:** Given the particular energy-maximising performance objective, wave energy converter (WEC) systems are prone to exhibit highly nonlinear behaviour. We present, in this paper, a detailed dynamic analysis and control synthesis for the Inertial Sea Wave Energy Converter (ISWEC) system, deriving and considering a comprehensive associated nonlinear model. In particular, we adopt a harmonic balance (HB) method to achieve this objective, producing the so-called amplitude-frequency curves (AFC) for the corresponding ISWEC nonlinear model, derived via a Lagrangian approach. We demonstrate that the system can present a variety of different behaviours which are completely neglected by its linear model counterpart. Leveraging both the efficiency, and convenient representation of the HB method, we synthesise so-called ‘passive’ (*i.e.* proportional) energy-maximising controllers using a variety of input conditions. We provide a comparison of the obtained control parameters with those arising from standard linear modelling, showing a consistent improvement in performance by effectively considering the relevant nonlinear ISWEC dynamics.

*Keywords:* Modeling, Wave energy converters, Application of nonlinear analysis and design, Modeling for control optimization, Energy systems

---

## 1. INTRODUCTION

Harnessing the high density power of the ocean is a clean, innovative, and sustainable way to curtail carbon pollution. Developing and up-scaling tailored technologies, such as wave energy converter (WEC) systems, represents a significant challenge. For this purpose, high fidelity models can help estimate the device performance and energy conversion capability. As such, availability of accurate, yet computationally efficient, models, represents a fundamental tool for a variety of optimization procedures, aiming at improving the performance of WEC systems within real scenarios (Windt et al., 2018; Faedo et al., 2020; Giorgi et al., 2021).

One particularly relevant application, which virtually always requires a parsimonious model, *i.e.* with a suitable trade-off between accuracy and computational demand, is the development of so-called energy-maximising control technology. Control systems for WEC devices aim at maximising the energy absorbed from the incoming wave field, hence directly contributing in lowering the associated cost of energy (Faedo et al., 2021). Given the (often significant) computational burden required by such strategies, researchers tend to consider overly simplified *linear* WEC models, aiming at alleviating the cost associated with real-time control implementation. Nonetheless, as demonstrated in *e.g.* (Ringwood et al., 2019), such

controllers can be particularly sensible to modelling errors: the infinitesimal motion assumptions, used to derive such linear WEC models, are potentially violated by the controller itself, which often requires large device motion to effectively maximise energy extraction.

Among the available WEC energy extraction technologies, a well-developed concept is that presented in the so-called *inertial sea wave energy converter* (ISWEC) (Bracco et al., 2011). The ISWEC is a self-referenced inertial-based floating WEC, which harvests the wave-induced motion on the floater to activate a resonant gyroscope connected to an electric generator. Nonetheless, virtually all studies regarding dynamic analysis and control of the ISWEC technology (apart from notable exceptions *e.g.* see (Novo et al., 2018)) consider linear models, hindering the highly nonlinear characteristics of this pitching system, and hence potentially providing inconsistent controller parameterisations and performance values.

Motivated by the discussion above, we provide, in this paper, a detailed dynamical analysis and control synthesis for the ISWEC system, deriving and considering a comprehensive nonlinear structure. In particular, we derive the corresponding nonlinear model using a Lagrangian approach, and adopt a harmonic balance (HB) method to analyse the resulting dynamical model (see *e.g.* (Krack and Gross, 2019)), producing the so-called amplitude-frequency curves (AFC) for the corresponding ISWEC dynamics. Note that, unlike (Novo et al., 2018), which con-

---

<sup>1</sup> Corresponding author - e-mail: [fabio.carapellese@polito.it](mailto:fabio.carapellese@polito.it).

siders only simulation studies with a simplified model, we demonstrate herein that the ISWEC system can present a variety of different dynamical phenomena which are completely neglected by its linear model counterpart, including *e.g.* bi-stability. Furthermore, leveraging the efficiency and convenient representation of the HB method, we synthesise so-called ‘passive’ (*i.e.* proportional) energy-maximising controllers using a variety of input conditions. We provide a comparison of the obtained control parameters with those arising from linear modelling, showing a consistent improvement in performance by effectively considering the relevant nonlinear ISWEC dynamics.

The remainder of this paper is organised as follows. Section 2 derives the nonlinear ISWEC model considered, also including a formal presentation of the adopted HB procedure. Section 3 presents a dynamical analysis of the ISWEC system, based upon the introduced model, while Section 4 provides both control synthesis based upon HB procedures, and consequent performance of the controlled system in terms of energy absorption. Finally, the conclusions of our study are elucidated in Section 5.

## 2. ISWEC MODEL

The ISWEC device is essentially composed of a gyroscopic system, mounted inside a floating hull, as in Figure 1. The floater pitch motion ‘activates’ the gyroscopic system, which hence oscillates, according to an angle  $\varepsilon : t \mapsto \varepsilon(t)$ , due to the forces generated by the incoming wave field. Note that, it is well-known (see *e.g.* (Townsend and Sheno, 2013)) that a gyroscopic system is parametrically excited if it is induced to rotate with respect to the set of axes defined by the reference frame  $\overrightarrow{Gxyz}$ . Such gyroscopic motion is then converted into electrical energy by means of a dedicated power take-off (PTO) actuator system.

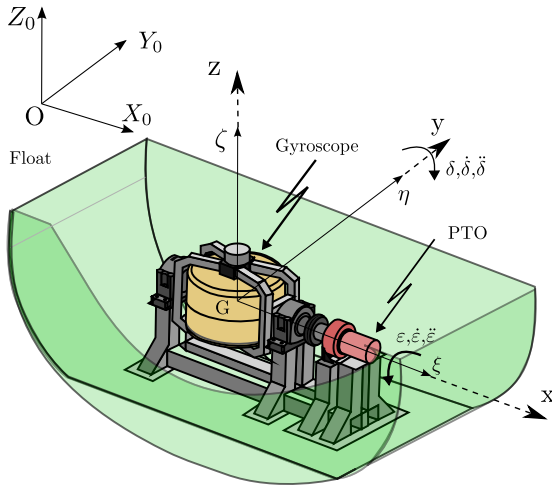


Fig. 1. Schematic representation of the ISWEC device

With respect to the floater hydrodynamics, we assume that the ISWEC system is allowed to rotate with respect to its  $y$ -axis, with a pitch rotation  $\delta : t \mapsto \delta(t) \in \mathbb{R}$  (as in *e.g.* (Bracco et al., 2011)). Note that, as described in (Bonfanti et al., 2020), we consider a recall mass  $m_p$ , mounted under the gyroscope gimbal at a proper distance  $l_p$  from the precession axis  $\xi$ , which results in an elastic effect due to gravity, as a reactive component in the system.

### 2.1 Nonlinear mechanical model

We derive, in this section, the fundamental nonlinear mathematical model describing the dynamics of the ISWEC device. In particular, we compute the full nonlinear equation of motion of the gyroscope, including the recall mass excited with respect to the floater  $y$ -axis. To begin with an appropriate definition of such a model, we define the corresponding reference frames describing ISWEC:

- $\overrightarrow{OX_0Y_0Z_0}$  is the inertial reference frame,
- $\overrightarrow{Gxyz}$  is the hull fixed reference frame,
- $\overrightarrow{G\xi\eta\zeta}$  is the gyroscope fixed reference frame.

Let  $q : t \mapsto q(t) \in \mathbb{R}^2$ , with  $q(t) = [\delta(t) \ \varepsilon(t)]^T$ , be the generalized motion vector. We can obtain the corresponding equation of motion for the ISWEC system by means of the Lagrange equations in terms of  $q$ , *i.e.*

$$\frac{d}{dt} \frac{\partial \mathcal{T}}{\partial \dot{q}} - \frac{\partial \mathcal{T}}{\partial q} + \frac{\partial \mathcal{U}}{\partial q} = \frac{\partial D}{\partial \dot{q}}, \quad (1)$$

where  $\mathcal{T}(q, \dot{q}) \in \mathbb{R}$  and  $\mathcal{U}(q) \in \mathbb{R}$  are the system kinetic and potential energy, respectively. The map  $D$  in (1) denotes the Rayleigh’s dissipation function, defined as

$$D(\dot{q}) = \frac{1}{2} \dot{q}^T c_{\text{tot}} \dot{q}, \quad (2)$$

where  $c_{\text{tot}} \in \mathbb{R}^{2 \times 2}$  is the corresponding damping matrix, defined as

$$c_{\text{tot}} = \begin{bmatrix} 0 & 0 \\ 0 & c_{\text{fric}} + c_{\text{PTO}} \end{bmatrix}, \quad (3)$$

where  $c_{\text{PTO}} \in \mathbb{R}^+$  is the (PTO) control parameter, adjusted to maximise energy conversion according to each corresponding sea state (see Section 4), and  $c_{\text{fric}} \in \mathbb{R}^+$  is the constant friction coefficient due to the sliding and rolling component of the precession shaft on the support bearings. The total angular velocity in the gyroscope reference frame of the gimbal  $[\omega_\xi \ \omega_\eta \ \omega_\zeta]^T$ , and the flywheel system  $[\Omega_\xi \ \Omega_\eta \ \Omega_\zeta]^T$ , are defined in terms the pitch floater velocity projection, and the angular velocity of the mechanism  $\dot{\varepsilon}$ , *i.e.*

$$\begin{aligned} \omega_\xi &= \dot{\varepsilon}, & \omega_\eta &= \dot{\delta} c_\varepsilon, & \omega_\zeta &= -\dot{\delta} s_\varepsilon, \\ \Omega_\xi &= \omega_\xi, & \Omega_\eta &= \omega_\eta, & \Omega_\zeta &= \omega_\zeta + \dot{\varphi}, \end{aligned} \quad (4)$$

where, from now on, the notation  $c_\alpha$  and  $s_\alpha$ , with  $\alpha \in \mathbb{R}$ , stands for  $\cos \alpha$  and  $\sin \alpha$ , respectively. Moreover, note that the flywheel and the gimbal have a zero linear velocity vector, since we have assumed that the floater is exclusively excited in pitch, and that the center of mass of both bodies and the floater coincide. In contrast, the pendulum mass has a non-zero linear velocity vector  $[v_\xi \ v_\eta \ v_\zeta]^T$  with respect to the  $\overrightarrow{G\xi\eta\zeta}$  frame, defined in terms of the pendulum arm  $l_p$  as

$$v_\xi = -l_p \dot{\delta} c_\varepsilon, \quad v_\eta = l_p \dot{\varepsilon}, \quad v_\zeta = 0. \quad (5)$$

We now subsequently define the corresponding inertia matrix of each subsystem characterising the ISWEC device as follows:

$$\begin{aligned} I_s &= \text{diag}(I_{s,x}, I_{s,y}, I_{s,z}), & I_f &= \text{diag}(I_{f,x}, I_{f,y}, I_{f,z}), \\ I_p &= \text{diag}(I_{p,x}, I_{p,y}, I_{p,z}), & I_h &= \text{diag}(I_{h,x}, I_{h,y}, I_{h,z}), \end{aligned} \quad (6)$$

where  $\{I_s, I_p, I_f\} \subset \mathbb{R}^{3 \times 3}$  are the inertia matrix of the gimbal, recall mass, and flywheel system, respectively, while  $I_h \in \mathbb{R}^{3 \times 3}$  is the inertia matrix of the hull. With the definitions provided up until this point, the nonlinear

equation, which fully describes the motion of the gyroscope system with respect to the precession axis, is given by

$$\begin{bmatrix} I_3 & 0 \\ 0 & I_1 \end{bmatrix} \begin{bmatrix} \ddot{\delta} \\ \ddot{\varepsilon} \end{bmatrix} = \begin{bmatrix} f_{\varepsilon\delta} \\ f_{\delta\varepsilon} + T_{\text{PTO}} \end{bmatrix}, \quad (7)$$

where

$$\begin{aligned} f_{\varepsilon\delta} &= -2I_2\dot{\delta}\dot{\varepsilon}c_\varepsilon s_\varepsilon + I_{f,z}\dot{\varphi}\dot{\varepsilon}c_\varepsilon - m_p l_p g c_\varepsilon^2 s_\delta, \\ f_{\delta\varepsilon} &= -c_{\text{fric}}\dot{\varepsilon} + I_2\delta^2 c_\varepsilon s_\varepsilon - I_{f,z}\dot{\varphi}\dot{\delta}c_\varepsilon - m_p l_p g s_\varepsilon c_\delta, \\ T_{\text{PTO}} &= -c_{\text{PTO}}\dot{\varepsilon}, \end{aligned} \quad (8)$$

and the inertia terms  $\{I_1, I_2, I_3\}$  in (7)-(8) are defined as

$$\begin{aligned} I_1 &= I_{s,x} + I_{f,x} + I_{p,x} + m_p l_p^2, \\ I_2 &= I_{s,z} + I_{f,z} + I_{p,z} - I_{g,y} - I_{s,y} - I_{p,y} - m_p l_p^2, \\ I_3 &= I_{h,y} + (I_{g,y} + I_{p,y} + I_{s,y} + m_p l_p^2)c_\varepsilon^2 \\ &\quad + (I_{g,z} + I_{p,z} + I_{s,z})s_\varepsilon^2, \end{aligned} \quad (9)$$

with  $g$  the acceleration due to gravity.

## 2.2 Hydrodynamic model

With the assumption that the fluid is inviscible and incompressible, and the fluid flow is irrotational, the so-called *linear potential flow theory* (Falnes, 2002) provides an approximation of the fluid-structure interaction through a time-domain system of Volterra integro-differential equations, written as

$$\Sigma : \{I_3\ddot{\delta} = f_w + f_h + f_r + f_{\varepsilon\delta}, \quad (10)$$

where  $f_w : \mathbb{R}^+ \rightarrow \mathbb{R}$  defines the (uncontrollable) wave excitation force,  $f_r : \mathbb{R}^+ \rightarrow \mathbb{R}$  is the so-called the radiation force, and  $f_h : \mathbb{R}^+ \rightarrow \mathbb{R}$  describes the hydrostatic restoring force acting on the floater. Such a force is defined proportional to the device (pitch) motion, and can be hence written as  $f_h = -S_h\delta$ , where  $S_h \in \mathbb{R}$  is the so-called hydrostatic stiffness coefficient.

The radiation force  $f_r$  is modelled using the well-known Cummins' equation, *i.e.*

$$f_r(t) = -\left(m^\infty\dot{\delta}(t) + \int_{\mathbb{R}^+} h_r(t-\tau)\dot{\delta}(\tau)d\tau\right), \quad (11)$$

where the first term in the summation, proportional to the device acceleration in pitch, corresponds to an inertial increase due to the water displaced when the body moves, while the second term corresponds with the dissipative force, proportional to the body velocity. In particular,  $m^\infty$  represents the so-called added-mass at infinite frequency, given by the relation  $m^\infty = \lim_{\omega \rightarrow +\infty} A_r(\omega)$ , where  $A_r(\omega)$  is the so-called frequency-dependent added-mass coefficient (see Falnes (2002)).

## 2.3 Coupled mechanical-hydrodynamic model

Within this section, we provide the coupled mechanical-hydrodynamic model  $\Sigma$ , by considering the inherent mechanical coupling between the gyroscope and the floater, and the hydrodynamic (pitch) motion of the device activated by the wave input force, *i.e.*

$$\Sigma : \left\{ \ddot{q} = \begin{bmatrix} \ddot{\delta} \\ \ddot{\varepsilon} \end{bmatrix} = \begin{bmatrix} f_w + f_h + f_r + f_{\varepsilon\delta} \\ f_{\delta\varepsilon} + T_{\text{PTO}} \end{bmatrix} \right\}. \quad (12)$$

For the sake of completeness, and given the comparison study provided in Sections 3 and 4, we provide, in the

following, the definition of a linear approximation of  $\Sigma$ . In particular, considering a small oscillation of the gyroscope about the equilibrium position  $(\varepsilon, \delta) = (0, 0)$ , the ISWEC dynamics  $\Sigma$  in (12) can be approximated in terms of the following linear structure:

$$\tilde{\Sigma}_l : \left\{ \ddot{q} = \begin{bmatrix} \ddot{\delta} \\ \ddot{\varepsilon} \end{bmatrix} = \begin{bmatrix} f_w + f_h + f_r + I_{f,z}\dot{\varphi}\dot{\varepsilon} \\ -I_{f,z}\dot{\varphi}\dot{\delta} - m_p g l_p \varepsilon + T_{\text{PTO}} \end{bmatrix} \right\}. \quad (13)$$

Finally, note that, given the nonlinear model  $\Sigma$  in (12), and considering the (passive) control PTO force  $T_{\text{PTO}} = -c_{\text{PTO}}\dot{\varepsilon}$  (as defined in equation (8)), we can compute the total absorbed mechanical power  $P_a$  for a given time interval  $\Xi = [0, T] \subset \mathbb{R}^+$  as

$$P_a = \frac{1}{T} \int_{\Xi} c_{\text{PTO}}\dot{\varepsilon}(t)^2 dt = \frac{1}{T} \int_{\Xi} P_i(t) dt, \quad (14)$$

where  $T$  corresponds to the wave period, and  $P_i = c_{\text{PTO}}\dot{\varepsilon}^2$  is the associated instantaneous mechanical power.

## 2.4 Harmonic Balance approach

Harmonic balance (HB) is a widely used technique for dynamic analysis of nonlinear systems, such as the ISWEC device presented in (12), and is based upon an approximate harmonic representation of the corresponding system variables (Krack and Gross, 2019). In this section, we briefly describe the particular HB implementation considered in our paper, which is based upon the theory presented in *e.g.* (Giorgi and Faedo, 2022).

We begin by noting that equation (12) can be re-written in terms of a continuous-time, state-space, system, defining the dynamics of the ISWEC device such that

$$\Sigma : \{ \dot{x} = f(x, f_{ex}), \quad (15)$$

where  $x(t) = [q(t)^T \dot{q}(t)^T]^T \in \mathbb{R}^n$ , with  $q$  as in equation (1) and, hence,  $n = 4$ , denotes the state-vector of (15),  $f_{ex}(t) = f_w(t) \in \mathbb{R}$  represents the forcing term, and  $f : \mathbb{R}^n \times \mathbb{R} \rightarrow \mathbb{R}^n$  is the corresponding state-transition map (which can be straightforwardly derived from (12)). The forcing function  $f_{ex}$  is considered as a trigonometric polynomial with a given amplitude  $F_{ex} \in \mathbb{R}^+$  and associated fundamental frequency  $\omega \in \mathbb{R}^+$ , *i.e.*

$$f_{ex}(t) = F_{ex} c_{\omega t}, \quad (16)$$

where, from now on, we refer to  $T = 2\pi/\omega$  as the fundamental period of (16). As per standard harmonic balance theory, we assume the (steady-state) solution of (15) can be approximated in terms of a finite-dimensional space  $\mathcal{H} = \text{span}(\mathcal{X})$ , with

$$\mathcal{X} = \{c_{p\omega t}, s_{p\omega t}\}_{p=1}^N, \quad (17)$$

where the set  $\mathcal{X}$  is complete, and  $\mathcal{H} \subset L^2(\Omega)$ , with  $\Omega = [0, T] \subset \mathbb{R}^+$ . To be precise,  $x_i \approx \tilde{x}_i$ , where  $\tilde{x}_i \in \mathcal{H}$ , can be expanded in terms of a linear combination of the elements composing  $\mathcal{X}$ , *i.e.*

$$\tilde{x}_i(t) = \sum_{p=1}^N \alpha_i^p c_{p\omega t} + \beta_i^p s_{p\omega t}, \quad (18)$$

with  $i \in \mathbb{N}_n$ , and  $\{\alpha_i^p, \beta_i^p\}_{p=1}^N \subset \mathbb{R}$ . To provide a compact representation of (18), let us define the auxiliary variables

$$\begin{aligned} \bar{X}_i &= [\alpha_i^1 \beta_i^1 \dots \alpha_i^N \beta_i^N], \\ \Upsilon(t) &= [c_{\omega t} s_{\omega t} \dots c_{N\omega t} s_{N\omega t}]^T \end{aligned} \quad (19)$$

where  $\{\bar{X}_i^\top, \Upsilon(t)\} \subset \mathbb{R}^N, \forall i \in \mathbb{N}_n$ , and hence the approximation  $\tilde{x}$  of the full state-vector can be written as

$$\tilde{x}(t) = \begin{bmatrix} \bar{X}_1^\top & \dots & \bar{X}_n^\top \end{bmatrix}^\top \Upsilon(t). \quad (20)$$

Furthermore, note that  $f_{ex}$  in (16) can also be written in terms of  $\Upsilon$  by use of an appropriate inclusion map, *i.e.*

$$f_{ex}(t) = F_{ex} c_{\omega t} = [F_{ex} \ 0] \Upsilon(t) = \bar{F} \Upsilon(t), \quad (21)$$

with  $\bar{F}^\top \in \mathbb{R}^N$ .

Let us now define the so-called residual function  $\mathcal{R}$  as

$$\mathcal{R}(\bar{X}, \bar{F}, \Upsilon) \equiv \dot{\tilde{x}} - f(\tilde{x}, f_{ex}) = \bar{X} \dot{\Upsilon} - f(\bar{X} \Upsilon, \bar{F} \Upsilon), \quad (22)$$

and let  $\mathcal{D}_c = \{\delta(t - t_j) = \delta_j\}_{j=1}^q \subset \Omega$ , with  $q > nN$ , be a set of shifted generalised Dirac-delta functions. Using the standard inner product in  $L^2(\Omega)$ , the expansion coefficients  $\bar{X}$ , defining the approximating solution  $\tilde{x}$ , can be computed via a Galerkin (pseudospectral) approach, where the projection of the residual function (22) onto the set  $\mathcal{D}_c$  is forced to be zero, *i.e.*

$$\langle \mathcal{R}, \delta_j \rangle = 0, \quad (23)$$

for  $j \in \mathbb{N}_q$ . Note that, as long as  $f \in \mathcal{C}$  in  $\Omega$ , for any fixed  $\bar{F}$ , the set of algebraic equations in (23) can be written in a compact form as

$$\bar{\mathcal{R}}(\bar{X}) = \begin{bmatrix} \bar{X} \dot{\Upsilon}(t_1) - f(\bar{X} \Upsilon(t_1), \bar{F} \Upsilon(t_1)) \\ \vdots \\ \bar{X} \dot{\Upsilon}(t_N) - f(\bar{X} \Upsilon(t_N), \bar{F} \Upsilon(t_N)) \end{bmatrix} = 0. \quad (24)$$

By way of example, and to provide a graphical appraisal of the solution computed via the adopted HB method, Figure 2 shows time-domain snippets for  $\varepsilon$  and  $\hat{\varepsilon}$ , computed according to the nonlinear model (12), using a time-advancing Runge-Kutta (RK) scheme (solid line), and the corresponding solution via HB with  $N = 15$  (dashed line). It can be appreciated that, after the transient period extinguishes, both solutions are virtually identical, effectively illustrating the validity of the proposed HB approach in reconstructing the steady-state response of (12).

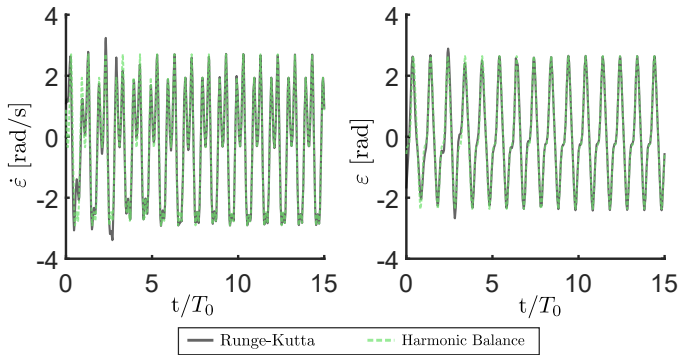


Fig. 2. Time-domain comparison of solutions computed via a time-advancing scheme (Runge-Kutta), and the approximating steady-state response via HB.

### 3. AMPLITUDE-FREQUENCY CURVE DEFINITION

We present, in this section, the so-called amplitude-frequency curves (AFC) for the nonlinear ISWEC model derived in Section 2. We begin by providing the corresponding definition of ‘amplitude’ in terms of the HB procedure described in Section 2.4.

In particular, throughout this section, we set  $N = 1$  in (18), *i.e.* we consider the same input frequency  $\omega$  for the approximation of the state variables associated with the ISWEC system and, consequently, for the definition of the residual equation in (24). Furthermore, we analyse the dynamics of the device in uncontrolled conditions, *i.e.* with  $c_{PTO} = 0$ , so as to: a) demonstrate the intrinsic nonlinear behaviour of the ISWEC system, and b) provide an open-loop AFC of the system, which can be used a-posteriori for control design purposes following (Faedo et al., 2022).

For the subsequent analysis, we focus on pitch and gyroscope displacement, *i.e.* the variables  $\delta = x_1$  and  $\varepsilon = x_2$ . We can now provide a definition of amplitude as a function of the input frequency as follows: Given an excitation input  $f_{ex}$  with frequency  $\omega$  and amplitude  $F_{ex}$  (as in (16)), and the corresponding HB solution for  $N = 1$ , we define the associated set of amplitudes  $\{\bar{\delta}, \bar{\varepsilon}\} \subset \mathbb{R}^+$  as

$$\begin{aligned} \bar{\delta} &= \max|\tilde{x}_3| = \sqrt{\alpha_3^2 + \beta_3^2}, \\ \bar{\varepsilon} &= \max|\tilde{x}_4| = \sqrt{\alpha_4^2 + \beta_4^2}. \end{aligned} \quad (25)$$

Based upon the amplitude definition provided in (25), Figure 3 shows the so-called AFC for both  $\varepsilon$  and  $\delta$ , normalised in terms of each corresponding input amplitude  $F_{ex}$ . Note that such input amplitude, which effectively depends upon the chosen frequency  $\omega$ , is computed in terms of the so-called excitation force kernel (see *e.g.* (Falnes, 2002)), taking into consideration a unitary free-surface elevation. Furthermore, note that Figure 3 also includes the amplitude boundaries  $\{\varepsilon_{con}, \delta_{con}\}$  corresponding to the maximum allowed values for  $\varepsilon$  and  $\delta$ , respectively, imposed by intrinsic physical limitations of the device components.

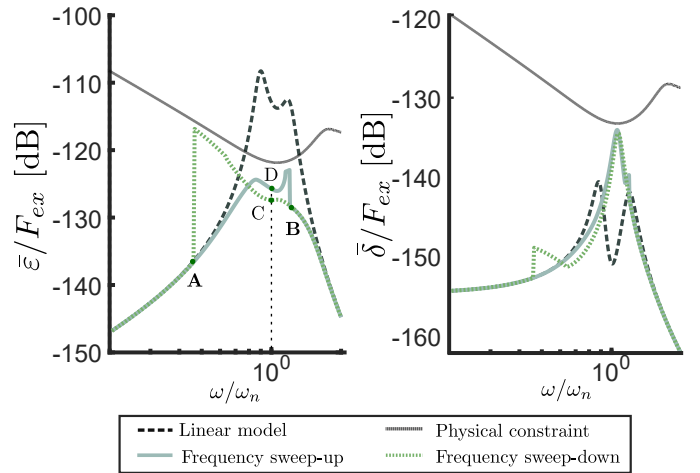


Fig. 3. AFC of the (uncontrolled) ISWEC referred to the PTO axis (left) and floater pitch motion (right).

The AFC plots presented in Figure 3 are computed based upon both a sweep-up (solid-grey line) and sweep-down (dashed-green line) frequency-dependent procedure: in the case of the former, the HB procedure is initiated from the lowest frequency component considered, and its associated solution is used as a starting point for the following (up) frequency, until the highest frequency value studied is reached. The latter is performed analogously, but in the opposite sense. As can be appreciated in Figure 4, the linear model effectively over-estimates the gyroscope

precession oscillation and, for the range of frequency close to the gyroscope natural frequency  $\omega_n$ , the amplitude of the response surpasses the limit value set by  $\varepsilon_{con}$ .

In the considered (uncontrolled) conditions, the ISWEC nonlinear system exhibits different dynamical behaviour for the sweep-up and sweep-down HB procedures. In particular, multi-stability exists within the frequency range delimited by points **A** and **B** in Figure 3. By way of example, and focusing at the natural frequency of the system, two solutions, indicated with points C and D, can be derived via the considered HB procedure. As illustrated in Figure 4, this indicates that two different solutions co-exist for the considered input signal, depending on the initial condition of system (12). In particular, Figure 4 (top) shows the steady-state solution for system (12), and its associated phase-portrait, corresponding with point C in Figure 3, while the solution presented in Figure 4 (bottom) corresponds to point D in Figure 3.

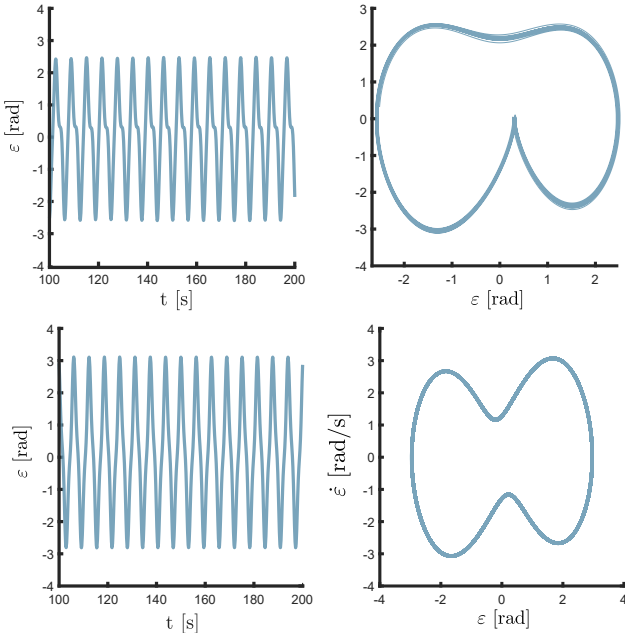


Fig. 4. Phase portraits representing the bi-stable condition of the ISWEC device.

#### 4. PERFORMANCE ASSESSMENT

Based upon the dynamic analysis provided in Section 3, we now analyse the performance of the device in terms of gyroscope rotation  $\bar{\varepsilon}$ , and corresponding output power, as a function of the normalized input frequency and (scaled) PTO damping  $c_0 = c_{PTO}/c_{opt}$ , where  $c_{opt}$  denotes the optimal damping value for each analysed frequency. Figure 5 presents an appraisal of the rotation performance, evaluated in terms of two key indicators:  $\varepsilon_0$ , which corresponds to the ratio between  $\bar{\varepsilon}$  and the maximum allowed rotation  $\varepsilon_{con}$ , and  $P_{a0}$ , which denotes the absorbed power  $P_a$  (as in (14)) scaled by the maximum power achieved within the presented analysis.

Note that the linear model consistently overestimates both the device motion, and the system performance, having a direct impact on the optimal control parameter  $c_0$ . Furthermore, the maximum power achievable according

to the linearised model, while respecting the corresponding motion constraints in  $\varepsilon_0$ , is effectively higher than the output power evaluated through the actual nonlinear model, resulting in a optimal damping value at resonance which is almost half of that arising from the corresponding nonlinear model. Therefore, the control parameters computed based upon the linear ISWEC model can lead to severely suboptimal results in terms of energy-maximising performance, when applied to the actual fully nonlinear system. At this point, it is worth to highlight that, unlike the uncontrolled case presented in Section 3, the nonlinear ISWEC model converges to the same AFC when controlled via its corresponding optimal energy-maximising damping, independently from the HB sweep direction.

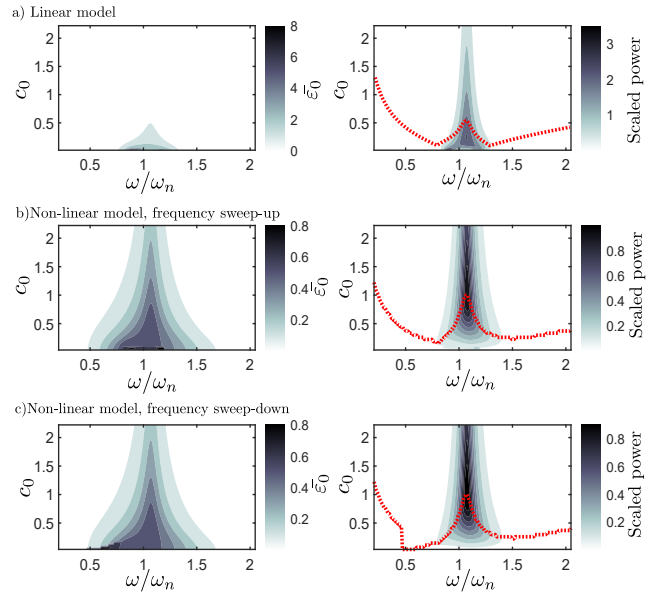


Fig. 5. Contour plot of the scaled rotation  $\varepsilon_0$  (left column) and scaled power (right column) as a function of  $\omega/\omega_n$  and  $c_0$ . The dashed line represents the optimal energy-maximising damping for each frequency.

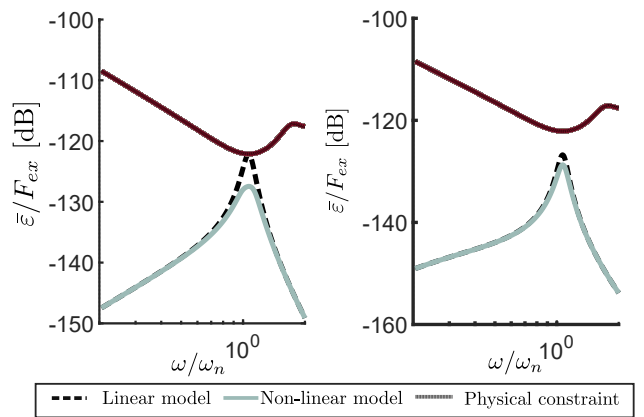


Fig. 6. Amplitude-frequency curve considering the optimal control parameter  $c_{PTO}$  derived from the linear model (left) and nonlinear model (right).

Figure 6 shows the AFC for the ISWEC system when applying the optimal damping derived from Figure 5 at the natural frequency of the system, *i.e.* when  $\omega/\omega_n = 1$ , for both linear, and nonlinear system models. In both cases,

the behaviour of the nonlinear model seems to approach the linear behaviour, since the damping somewhat ‘alleviates’ the main nonlinear effects acting on the system. Nonetheless, the motion resulting from the linear model always presents an overestimation with respect to the realistic nonlinear dynamics.

Figure 7 shows time-series of scaled velocity of the gyroscope  $\dot{\xi}_0$ , and scaled instantaneous power  $P_{i0}$ . Such signals are compared considering different  $c_{PTO}$  parameters, defined in terms of both the linear ISWEC model, and the corresponding fully nonlinear system. In the case of the latter, we determine two different optimal control parameters  $c_0$ : one optimised via HB considering only the first input harmonic ( $N = 1$ ), and the second parameter obtained via optimization on the fully non-linear model, simulated in time-domain via RK. The maximum mean power value, represented in terms of horizontal lines in Figure 7 (right), is obtained via the optimal damping derived from the time-domain RK approach. We do note, although, that the optimal PTO damping computed via HB with  $N = 1$  provides a good compromise for controller design, given that the mean power obtained is effectively very close to that computed via RK (which requires a full solution of the nonlinear differential equation (12)). Finally, note that the PTO damping value, computed using the linear ISWEC model, effectively overestimates the system response, leading to suboptimal control parameters.

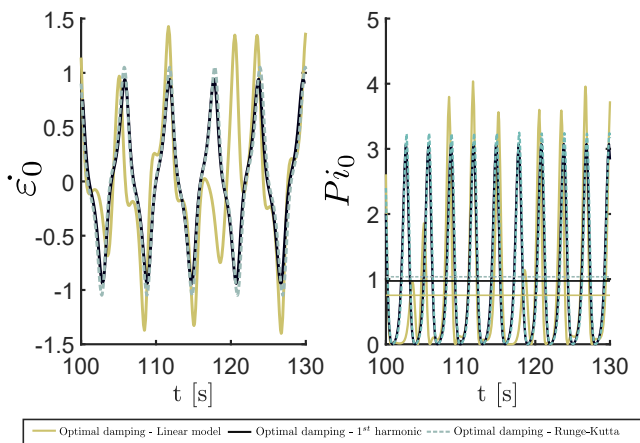


Fig. 7. Time series of the scaled gyroscope velocity  $\dot{\xi}_0$  and the instantaneous power for different value of  $c_{PTO}$ .

## 5. CONCLUSION

Given the intrinsic nonlinear behaviour of the ISWEC system, we present, in this paper, the derivation and subsequent dynamic analysis of a comprehensive nonlinear model for such technology, including also appropriate a passive control synthesis procedure. Such objective is accomplished via a HB approach, where the nonlinear behaviour of the WEC is compared with respect to its linear modelling counterpart, highlighting a number of fundamental differences, which are shown to have an impact in control synthesis and performance assessment. In particular, we show that neglecting nonlinear behaviour can lead to a significant loss in power absorption capabilities, with control coefficients largely deviated from those which are optimal for the derived nonlinear model.

## REFERENCES

- Bonfanti, M., Carapellese, F., Sirigu, S., Bracco, G., and Mattiazzo, G. (2020). Excitation Forces Estimation for Non-linear Wave Energy Converters: A Neural Network Approach. *IFAC-PapersOnLine*, 53. doi:10.1016/j.ifacol.2020.12.1213.
- Bracco, G., Giorcelli, E., and Mattiazzo, G. (2011). ISWEC: A gyroscopic mechanism for wave power exploitation. *Mechanism and Machine Theory*, 46(10), 1411–1424. doi:10.1016/j.mechmachtheory.2011.05.012.
- Faedo, N., Carapellese, F., Pasta, E., and Mattiazzo, G. (2022). On the principle of impedance-matching for underactuated wave energy harvesting systems. *Applied Ocean Research*, 118. doi:10.1016/j.apor.2021.102958.
- Faedo, N., Dores Piuma, F.J., Giorgi, G., and Ringwood, J.V. (2020). Nonlinear model reduction for wave energy systems: a moment-matching-based approach. *Nonlinear Dynamics*, 102(3), 1215–1237. doi:10.1007/s11071-020-06028-0.
- Faedo, N., Scarciotti, G., Astolfi, A., and Ringwood, J.V. (2021). Nonlinear energy-maximizing optimal control of wave energy systems: A moment-based approach. *IEEE Transactions on Control Systems Technology*, 29(6), 2533–2547.
- Falnes, J. (2002). *Ocean Waves and Oscillating Systems*. Cambridge University Press. doi:10.1017/CBO9780511754630.
- Giorgi, G. and Faedo, N. (2022). Performance enhancement of a vibration energy harvester via harmonic time-varying damping: A pseudospectral-based approach. *Mechanical Systems and Signal Processing*, 165, 108331. doi:10.1016/j.ymsp.2021.108331.
- Giorgi, G., Sirigu, S., Bonfanti, M., Bracco, G., and Mattiazzo, G. (2021). Fast nonlinear Froude–Krylov force calculation for prismatic floating platforms: a wave energy conversion application case. *Journal of Ocean Engineering and Marine Energy*, 7(4), 439–457. doi:10.1007/s40722-021-00212-z.
- Krack, M. and Gross, J. (2019). *Harmonic balance for nonlinear vibration problems*, volume 1. Springer.
- Novo, R., Bracco, G., Sirigu, S.A., Mattiazzo, G., Mériçaud, A., and Ringwood, J.V. (2018). Non linear simulation of a wave energy converter with multiple degrees of freedom using a harmonic balance method. In *International Conference on Offshore Mechanics and Arctic Engineering*, volume 51319, V010T09A041. American Society of Mechanical Engineers.
- Ringwood, J.V., Mériçaud, A., Faedo, N., and Fusco, F. (2019). An analytical and numerical sensitivity and robustness analysis of wave energy control systems. *IEEE Transactions on Control Systems Technology*, 28(4), 1337–1348.
- Townsend, N.C. and Shenoi, R.A. (2013). Modelling and analysis of a single gimbal gyroscopic energy harvester. *Nonlinear Dynamics*, 72(1-2), 285–300. doi:10.1007/s11071-012-0713-7.
- Windt, C., Faedo, N., Penalba, M., and Ringwood, J. (2018). Evaluation of energy maximising control systems for the wavestar wave energy converter. In *Proceedings of the 2019 American Control Conference, Philadelphia, USA*, 4791–4796.